Continuous acquisition scanner for whole-body multispectral optoacoustic tomography

Rui Ma [a], Vasilis Ntziachristos [a], and Daniel Razansky*[a]
[a]Institute for Biological and Medical Imaging, Technical University of Munich and Helmholtz Center Munich, Ingolstädter Landstraβe 1, 85764 Neuherberg, Germany

ABSTRACT

An essential problem dealing with three-dimensional optoacoustic imaging is the long data acquisition times associated with recording signals from multiple spatial projections, where signal averaging for each projection is applied to obtain satisfying signal-to-noise-ratio. This approach complicates acquisition and makes imaging challenging for most applications, especially for in vivo imaging and multispectral imaging. Instead we employ a herein introduced continuous data acquisition methodology that greatly shortens recording times over multiple projection angles and acquires high quality tomographic data without averaging. By this means a two dimensional image acquisition having 270 angular projections only takes about 9 seconds, while a full multispectral three dimensional image can normally take about 15 minutes to acquire with a single ultrasonic detector. The system performance is verified on tissue-mimicking phantoms containing known concentrations of fluorescent molecular agent as well as small animals.

Keywords: Photoacoustic imaging, Biomedical Optics, Multispectral and hyperspectral imaging, Medical and biological imaging, Medical optics instrumentation

1. INTRODUCTION

Multispectral optoacoustic tomography (MSOT) is an imaging methodology that is able to resolve chromophoric and fluorescent agents with molecular specificity through several millimeters to centimeters of tissue[1, 2]. The technique is based on the optoacoustic phenomenon, i.e. the generation of acoustic waves due to thermoelastic expansion caused by absorption of ultra-short optical pulses. Over the last decade optoacoustics has been considered for tissue imaging, mainly for resolving vascular contrast and the corresponding physiological changes, in particular oxy- and deoxy-hemoglobin[3], superficial vascular anatomy[4], brain lesion and functional cerebral hemodynamic changes[5], cancer angiogenesis[6], blood volume and oxygen consumption changes and the associated dynamic and functional neuronal activities[7]. The introduction of endogenous or exogenous reporter agents with molecular specificity, such as fluorescent proteins and probes, further allows the propagation of this technique towards molecular imaging applications. In this case a promising approach is the use of multispectral illumination in order to differentiate specific spectral signatures of key reporter agents over the background tissue absorption[1, 2, 8-10]. Combined, imaging of physiological and molecular markers using optoacoustics has the potential to achieve high resolution photonic imaging, through depths that go significantly beyond the capabilities of modern microscopy[11, 12].

To perform molecular imaging of tissues and small biological organisms using MSOT, we developed an experimental prototype that is capable of fast multi-slice whole-body imaging using a single transducer. This system employs multi-angle side illumination of the entire volume of interest and introduces a so called continuous data acquisition method to replace the commonly used data averaging for each projection angle, which is time consuming and limits its application of exploring some dynamic and longitudinal phenomena that require good temporal resolution, such as dynamic bio-distribution of contrast agents, cell tracking, blood oxygenation monitoring etc.

*dr@tum.de; phone +49(0)-89-3187-1587; fax +49(0)-89-3187-3017; http://www.helmholtz-muenchen.de/en/ibmi/

Photons Plus Ultrasound: Imaging and Sensing 2010, edited by Alexander A. Oraevsky, Lihong V. Wang,
Proc. of SPIE Vol. 7564, 756429 · © 2010 SPIE · CCC code: 1605-7422/10/$18 · doi: 10.1117/12.842776

Downloaded From: http://proceedings.spiedigitallibrary.org/ on 08/02/2016 Terms of Use: http://spiedigitallibrary.org/ss/TermsOfUse.aspx

2. METHODS AND MATERIALS

2.1 Experimental setup

Fig. 1 displays a simplified sketch of the system. A tunable optical parametric oscillator (MOPO-700 series, Newport Corp., Mountain View, CA), pumped by a Q-switched Nd:YAG laser (Quanta-Ray Lab-Series 190-30 Newport), provides multi-wavelength illumination. The pulse duration of the laser is less than 10 ns and the repetition rate is 30Hz. The output laser beam is manipulated using an iris, slits, cylindrical/spherical lenses, and diffusers in order to improve illumination uniformity and adapt the incident beam shape to the size of the particular imaged object or region of interest. A beam splitter divides the beam into two equal-intensity parts illuminating the object's surface from opposite directions through two transparent windows in the water tank. In this way, excitation conditions close to uniform illumination are achieved. The laser pulse fluence on the surface of imaged objects is kept under 20 mJ/cm^2 in order to meet laser safety standards[13]. Optoacoustic signals are acquired using ultrasound transducers with central frequencies and focal lengths suited to the size of the imaged object and the scale of the features of interest. For smaller objects, such as the Drosophila pupa and Zebrafish presented herein, a piezoelectric PZT transducer with a 15 MHz central frequency, 19.05 mm focal length and 13 mm element diameter (V319, Panametrics-NDT, Waltam, MA) is used; larger tissue-mimicking phantoms, are imaged using a PZT transducer with a 3.5 MHz central frequency, 38.1 mm focal length and 13 mm element diameter (V382, Panametrics-NDT, Waltam, MA). The transducers are cylindrically focused in the imaging plane to facilitate 2D image acquisition.

We use two 45° tilted mirrors to change the beam height by moving the bottom mirror with a vertical translation stage. The beam splitter and the ultrasonic transducer are translated by the same stage, thus both the illumination and detection planes are translated simultaneously to allow for multi-slice image acquisition via vertical scanning. The sample is mounted on a rotational stage located at the bottom of the water tank while a sealed bearing (Isomag Corporation, Los Angeles, CA) is used to isolate the water-containing area from the stepper motor located underneath the tank. In-plane data acquisition is done by 360° rotation of the sample. This arrangement ensures a compact design as only a small number of necessary components are located inside the water tank. A 14-bit resolution PCI digitizer with a sampling rate of 100 MS/s (NI PCI-5122, National Instruments Corp., Austin, TX) is used to record time-resolved acoustic signals from the detector. The laser, stages, and data acquisition are controlled via a Labview-based interface (National Instruments Corp., Austin, TX). In addition, a photodiode (FDS010, 200-1100 nm, 1 ns rise time, Thorlabs, Newton, NJ) is positioned in the vicinity of the laser output window to record the intensity change of each pulse and normalize the detected signals for laser output instabilities. The readings from the photodiode are calibrated with wavelength-dependent sensitivity curves provided by the manufacturer. This continuous power monitoring is of critical importance for multispectral reconstructions since many important molecular imaging agents may present only a small variation of the optical absorption over highly absorbing background, in which case even small quantification inaccuracies may lead to uninterpretable results.

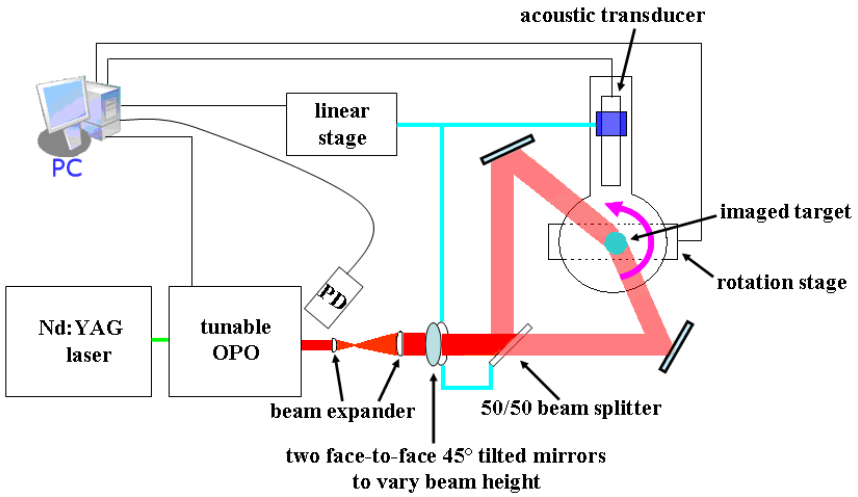

Fig. 1. Scheme of the multispectral optoacoustic tomography setup.

Downloaded From: http://proceedings.spiedigitallibrary.org/ on 08/02/2016 Terms of Use: http://spiedigitallibrary.org/ss/TermsOfUse.aspx

2.2 Phantom preparation

To evaluate the performance of the developed system, three turbid tissue-mimicking cylindrical phantoms labeled Ph1, Ph2 and Ph3, with optical properties as summarized in Table 1, were employed. Ph1 and Ph2 were made by molding 1.5% (by weight) of agar powder (Sigma-Aldrich, St. Louis, MO) mixed with 6% (by volume) of Intralipid-20% (Sigma-Aldrich, St. Louis, MO) to attain a reduced scattering coefficient of $\mu_s' = 10$ cm^{-1} and black India ink (Higgins, Sanford Bellwood, IL) for absorption. Hexagonal and round inclusions, with optical properties as in Table 1, were added to the phantoms. Ph3 was made of Polyvinyl chloride-plastisol (PVCP) with Titanium dioxide (TiO2) powder and black plastic color (BPC) to introduce the necessary scattering and absorption[9]. Hydrophobic PVCP was used in order to hold solutions of fluorescent dyes, which tend to diffuse through agar phantoms. Ph1-Ph3 were imaged using the 3.5 MHz PZT transducer described in Section 2.1. The background scattering and absorption properties of the phantoms were selected in the range of typical mouse tissue optical properties at the imaged wavelengths[9].

Table 1. Optical properties of the phantoms used for experimental validation.

Parameters \ Label	Ph1	Ph2	Ph3
Diameter (mm)	14	28.5	17
μ_s' background (cm^{-1})	10	10	20
μ_a background (cm^{-1})	0.2	0.8	0.15
μ_s' insertion/s (cm^{-1})	10	10	20
μ_a insertion/s (cm^{-1})	1	8	2*
* 5μM Texas Red was added to one of the insertions.			

2.3 Animal imaging preparation

A Drosophila melanogaster pupa and 1-year old adult Zebrafish *post mortem* were imaged using the 15 MHz PZT transducer described in *2.1* in order to resolve their relatively small features. These organisms have both significant scattering and relatively small size that prevents them from being visualized using any of the existing microscopic [11, 12] or macroscopic (diffusion-based)[14] optical tomography techniques. The organisms were either partially or fully embedded into clear agar cylinders for simple handling and tomographic rotation. The typical diameter of a Drosophila melanogaster pupa is approximately 800 μm and the case is very scattering and absorbing. We acquired optoacoustic data from a pupa in the region of the salivary glands at 498 nm using the selective-plane illumination technique[15]. An adult Zebrafish has a cross-sectional diameter of approximately 6 mm and is also optically diffuse. Here, a wavelength of 605 nm was used for illumination. As a demonstration of molecular imaging in small animals we imaged a transgenic Zebrafish *post mortem* with mCherry expressed in the brain area.

RESULTS

3.1 Turbid phantom images

Figure 2(a) show optoacoustic image of Ph1 using continuous acquisition with 270 angular projections without averaging. It takes approximately 9 seconds to acquire the 2D image. To simulate imaging of deep-seated targets in a very absorbing tissue-like medium, Ph2 was used with a diameter of 28.5mm. It was made with a background optical absorption coefficient of μa = 0.8 cm^{-1}, which is approximately four times higher than average mouse tissue absorption at the imaging wavelength of 650 nm. Figure 2(b) shows optoacoustic reconstructions of Ph2 acquired at 650nm containing a hexagonal insertion at a depth of more than 1 cm, which is clearly visible in the images with high resolution and SNR. Figure 2(c) shows a magnified view of the insertion from the image in Fig. 2(b). The calculated SNR of the image in Fig. 2(c) is 22.25 dB, where the green and magenta labeled regions represent signal and background respectively. The system has therefore been clearly demonstrated to have the capability of imaging deep tissue contrast within large objects with relatively high background absorption.

Downloaded From: http://proceedings.spiedigitallibrary.org/ on 08/02/2016 Terms of Use: http://spiedigitallibrary.org/ss/TermsOfUse.aspx

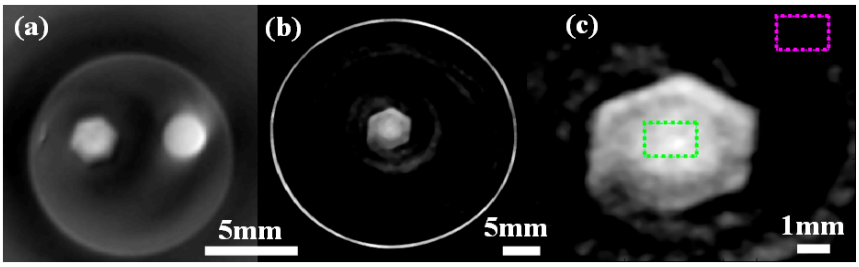

Fig. 2. (a) Optoacoustic reconstruction of Ph1 acquired in continuous acquisition mode with 270 angular projections; (b) Optoacoustic reconstruction of Ph3 acquired at 650nm; (c) Magnified image around the insertion. SNR is calculated from the green and magenta labeled regions, representing signal and background respectively.

3.2 Animal imaging

The image of the Drosophila pupa, shown in Fig. 2(a), clearly reveals the anatomical details of the animal, i.e. the absorbing case, two absorbing salivary glands and the rest of the volume filled with fatty structures. Fig. 2(b) displays the cross-sectional Zebrafish image and further demonstrates the high contrast and resolution capability of the system.

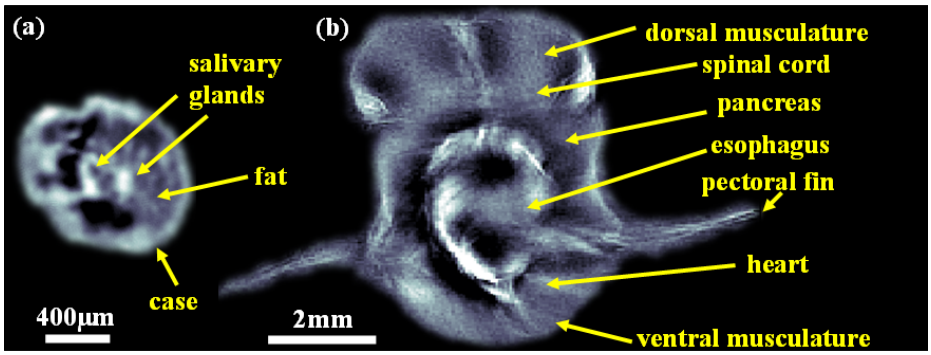

Fig. 3. (a) Optoacoustic image of intact drosophila pupa; (b) Cross-sectional optoacoustic image of an intact 1- year old adult Zebrafish.

3.3 Molecular imaging

As described in Section *2.2*, Ph3 was used to demonstrate system's molecular probe detection sensitivity. For this, the phantom was embedded with a solution containing a common fluorescent dye, Texas Red (peak excitation 596 nm; peak emission 615 nm) at 5 μM concentration. The dye was in an already highly absorbing solution of ink having $\mu_a = 2\text{cm}^{-1}$, which was selected in order to simulate the realistic case of a fluorescent imaging agent located in whole blood. We employed continuous data acquisition to obtain optoacoustic images at the peak excitation wavelength of Texas Red (596nm) and at 612nm where its absorption drops significantly [Fig. 4(a)-4(b)]. By subtracting optoacoustic images at these two wavelengths one can efficiently suppress the slowly varying background absorption and reveal the correct location of the Texas Red dye, as shown in Fig. 4(c).

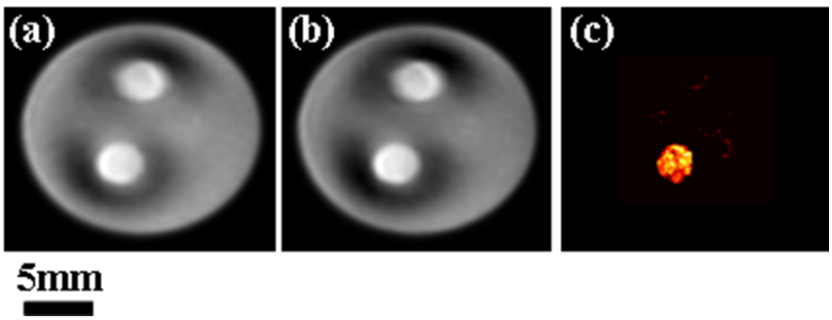

Fig. 4. Optoacoustic images of Ph3 acquired at (a) 596 nm and (b) 612 nm. (c) Subtraction between 596 nm and 612 nm images revealing location of the Texas Red dye.

Downloaded From: http://proceedings.spiedigitallibrary.org/ on 08/02/2016 Terms of Use: http://spiedigitallibrary.org/ss/TermsOfUse.aspx

As can be seen, the subtraction process reduces background signals coming from both insertions containing the highly absorbing ink solution and from the background of the phantom as well. We calculated the Contrast-to-noise ratio (CNR) of the multispectral image using the following formula:

$$CNR = \frac{S_{Dye} - S_B}{\sigma} \quad (1)$$

where S_{Dye} is the averaged value of dye signal obtained after wavelength subtraction [Fig. 4(c)], S_B is the averaged value of the background after wavelength subtraction, and σ is the standard deviation of S_B. The calculated SNR and CNR in Fig. 4(c) were 25.17 and 16.87, respectively, which translates to a noise floor equivalent dye concentration of ~300 nM. This translates to an amount of 12 femtomoles of the dye that was detected in each resolution-limited voxel of the 3.5 MHz PZT transducer (~0.2 x 0.2 x 1 mm). However, in our phantom experiment, the actual optoacoustic signals were recorded from a large amount of the dye contained in the insertion. As we have shown[9] the detection sensitivity limits cannot therefore be linearly extrapolated using measurements performed on larger amounts of the probe. A more accurate analysis based on the methodology[9], which takes into account optical properties, size and depth of the target as well as light and acoustic attenuation, will lead to detection limits on the order of several hundreds of femtomoles for the current experimental setup and phantom properties. Clearly, in realistic animal experiments, additional factors, such as absorption inhomogeneities, acoustic mismatches, movement artifacts and other issues related to in-vivo imaging, will adversely affect image quantification and sensitivity limits. There we expect for sensitivity limits in the few picomoles range, similar to what is achievable with state-of-the-art fluorescent molecular tomography systems[16].

Fig. 5 further demonstrates the capability of our system resolving fluorescent proteins in small animal imaging. The imaged object is an adult transgenic Zebrafish expresses mCherry in the brain area. We imaged the zebrafish at 585 nm and 615 nm and substracted the two images to get the location with mCherry expression. Fig. 4(a) is the reconstructed optoacoustic images that are zoomed in the brain area at 585 nm. From Fig. 4(b) we could clearly see the resolved mCherry expression. In Fig. 4(b) there are two other high absorbing areas in the diffuse nucleus of the inferior lobe and tectum opticum region, which is probably due to the arterial blood supply in these regions. This could be further verified by imaging fish without any expression.

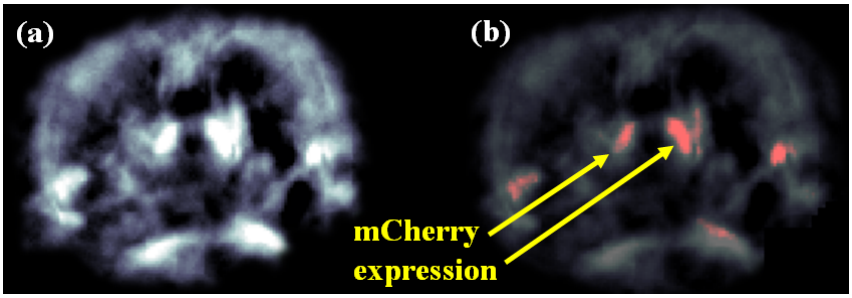

Fig. 5. Optoacoustic images of the brain of an adult transgenic Zebrafish acquired at (a) 585 nm and (b) Subtraction between 585 nm and 615 nm images resolving location of the mCherry expression, imposed on 585 nm optoacoustic image.

DISCUSSION AND CONCLUSIONS

The presented fast-acquisition multispectral optoacoustic tomography system for whole-body imaging of small animals enables compact tomographic design by using sealed bearing that effectively isolates liquid area from the rotation driving parts. The scanner provides a variety of optical means for optimal adjustment of sample excitation. This offers the flexibility required for imaging at different object dimension scales, from organisms like Drosophila pupa (diameter below 1 mm) up to larger animals and samples with characteristic sizes of few centimeters and more. The two-way illumination configuration is adopted for attaining approximate uniformity in object's illumination, which is crucial for high quality quantitative image reconstruction. To speed up the acquisition process, we employ a continuous acquisition methodology, for which the object is rotating constantly during data acquisition, a method that was shown to save up to one order of magnitude in typical acquisition times.

Downloaded From: http://proceedings.spiedigitallibrary.org/ on 08/02/2016 Terms of Use: http://spiedigitallibrary.org/ss/TermsOfUse.aspx

In its current implementation, the scanner is capable of acquiring a single wavelength 2D image in approximately 9 seconds using a single cylindrically-focused ultrasonic detector, which corresponds to acquisition times of about 20 minutes for typical whole-body multi-wavelength data acquisition using 40 vertical slices and 3 wavelengths. A cylindrically focused element is used here in order to increase detection area and sensitivity, in exchange for compromising image quality and resolution along dimensions where focusing is performed.

Furthermore, multi-wavelength illumination offers the possibility to resolve exogenously administered fluorescent probes or other chromophores. The simplest image subtraction approach, demonstrated here, works optimally with absorbers that offer a steep absorption (extinction) change, characteristic of fluorochromes. However, measurements at multiple wavelengths can provide further ability to simultaneously resolve multiple biomarkers, dyes and other intrinsic and exogenous chromophores.

ACKNOWLEDGMENT

D. R. acknowledges support from the German Research Foundation (DFG) Research Grant (RA 1848/1).

REFERENCES

1. Razansky, D., Distel, M., Vinegoni, C., Ma, R., Perrimon, N., Koster, R. W., and Ntziachristos, V., "Multispectral opto-acoustic tomography of deep-seated fluorescent proteins in vivo," Nature Photonics 3(7), 412-417 (2009).
2. Razansky, D., Vinegoni, C., and Ntziachristos, V., "Multispectral photoacoustic imaging of fluorochromes in small animals," Opt. Lett. 32(19), 2891-2893 (2007).
3. Zhang, H. F., Maslov, K., Sivaramakrishnan, M., Stoica, G., and Wang, L. H. V., "Imaging of hemoglobin oxygen saturation variations in single vessels in vivo using photoacoustic microscopy," Applied Physics Letters 90(5), 053901 (2007).
4. Zhang, E. Z., Laufer, J. G., Pedley, R. B., and Beard, P. C., "In vivo high-resolution 3D photoacoustic imaging of superficial vascular anatomy," Physics in Medicine and Biology 54(4), 1035-1046 (2009).
5. Wang, X. D., Pang, Y. J., Ku, G., Xie, X. Y., Stoica, G., and Wang, L. H. V., "Noninvasive laser-induced photoacoustic tomography for structural and functional in vivo imaging of the brain," Nature Biotechnology 21(7), 803-806 (2003).
6. Oraevsky, A. A., Andreev, V. A., Karabutov, A. A., Fleming, R. D., Gatalica, Z., Singh, H., and Esenaliev, R. O., "Laser optoacoustic imaging of the breast: detection of cancer angiogenesis," Proc. SPIE, 3597, 352-363 (1999).
7. Zhang, H. F., Maslov, K., Stoica, G., and Wang, L. H. V., "Functional photoacoustic microscopy for high-resolution and noninvasive in vivo imaging," Nature Biotechnology 24(7), 848-851 (2006).
8. Yuan, Z. and Jiang, H. B., "Simultaneous recovery of tissue physiological and acoustic properties and the criteria for wavelength selection in multispectral photoacoustic tomography," Opt. Lett. 34(11), 1714-1716 (2009).
9. Razansky, D., Baeten, J., and Ntziachristos, V., "Sensitivity of molecular target detection by multispectral optoacoustic tomography (MSOT)," Medical Physics 36(3), 939-945 (2009).
10. Zhang, E., Laufer, J., and Beard, P., "Backward-mode multiwavelength photoacoustic scanner using a planar Fabry-Perot polymer film ultrasound sensor for high-resolution three-dimensional imaging of biological tissues," Applied Optics 47(4), 561-577 (2008).
11. Helmchen, F. and Denk, W., "Deep tissue two-photon microscopy," Nature Methods 2(12), 932-940 (2005).
12. Yuste, R., "Fluorescence microscopy today," Nature Methods 2(12), 902-904 (2005).
13. American National Standards for the Safe Use of Lasers, ANSI Z136.1, American Laser Institute (2000).
14. Weissleder, Ralph and Ntziachristos, Vasilis, "Shedding light onto live molecular targets," Nat Med 9(1), 123-128 (2003).
15. Razansky, D., Vinegoni, C., and Ntziachristos, V., "Imaging of mesoscopic-scale organisms using selective-plane optoacoustic tomography," Physics in Medicine and Biology 54(9), 2769-2777 (2009).
16. Deliolanis, N., Lasser, T., Hyde, D., Soubret, A., Ripoll, J., and Ntziachristos, V., "Free-space fluorescence molecular tomography utilizing 360 degrees geometry projections," Opt. Lett. 32(4), 382-384 (2007).

Downloaded From: http://proceedings.spiedigitallibrary.org/ on 08/02/2016 Terms of Use: http://spiedigitallibrary.org/ss/TermsOfUse.aspx